

---

# A Gauge Theory of Superposition: Toward a Sheaf-Theoretic Atlas of Neural Representations

Hossein Javidnia

School of Computing

Dublin City University, Ireland

hossein.javidnia@dcu.ie

## Abstract

We develop a discrete gauge-theoretic framework for superposition in large language models (LLMs) that replaces the single-global-dictionary premise with a sheaf-theoretic atlas of local semantic charts. Contexts are clustered into a stratified context complex; each chart carries a local feature space together with a local information-geometric metric (Fisher/Gauss–Newton) that identifies which feature interactions are predictively consequential Amari (2016); Martens & Grosse (2015). This induces a Fisher-weighted interference energy and three geometric obstructions to global interpretability: **(O1) Local jamming** (active load exceeds Fisher bandwidth), **(O2) proxy shearing** (mismatch between geometric transport and a fixed correspondence proxy across overlaps), and **(O3) nontrivial holonomy** (path-dependent transport around loops).

We prove and empirically instantiate four results on a frozen open LLM (Llama 3.2 3B Instruct) using standard text and code corpora (WikiText-103 raw, a C4-derived English web-text subset, and `the-stack-smol`) Meta (2024); Merity et al. (2016); Raffel et al. (2020); Kocetkov et al. (2022). (A) A constructive spanning-tree gauge theorem shows that, after gauge fixing on a spanning tree, each chord residual equals the holonomy of its fundamental cycle, making holonomy computable and gauge-invariant. (B) Shearing lower-bounds a data-dependent transfer mismatch energy, turning  $D_{\text{shear}}$  into an unavoidable failure bound. (C) A non-vacuous certified jamming/interference bound holds on consequential atom subsets with high coverage and zero violations across random seeds and hyperparameters. (D) Bootstrap and sample-size experiments establish estimator stability for  $D_{\text{shear}}$  and  $D_{\text{hol}}$ , with improved concentration on persistent (well-conditioned) subsystems predicted by polar-factor perturbation theory Higham (1986); Schönemann (1966). Our framework supplies reproducible evaluation primitives for *when and why* global interpretability breaks, separating failures due to local overload (jamming), cross-chart mismatch (shearing), and intrinsically path-dependent transport (holonomy).

Code: [https://github.com/hosseinjavidnia/gauge\\_superposition](https://github.com/hosseinjavidnia/gauge_superposition)

## 1 Introduction

Mechanistic interpretability often assumes that a single feature dictionary can explain a layer uniformly across contexts Bereska & Gavves (2024); Conmy et al. (2023). However, both toy models of superposition and large-scale feature-learning results suggest that this premise can fail: representations may encode more features than ambient dimension by packing sparse directions, inducing interference and context-dependent feature identities Elhage et al. (2022); Bricken et al. (2023); Templeton et al. (2024). We therefore reframe the goal: interpretability should be treated as a *local-to-global* construction problem, where feature descriptions are locally coherent but may exhibit measurable obstructions to being glued into a single global account.

### 1.1 Contribution and paper thesis

We model the space of contexts by a stratified simplicial complex (implemented as a graph of context clusters), and we attach to each cluster a local feature space. Transitions between neighbouring clusters are

arXiv:2603.00824v1 [cs.LG] 28 Feb 2026

---

represented by *partial transports*; loop compositions define holonomy. The central thesis is that failures of global interpretability can be decomposed into three distinct obstructions (O1–O3) that are measurable from a frozen model.

To avoid ambiguity about what is proven versus what is measured, we isolate four results (A–D) that connect theory to experiments:

- **(A) Spanning-tree gauge identity.** After a constructive gauge fixing on a spanning tree, tree-edge defects vanish and each chord defect equals the holonomy of its fundamental cycle (Theorem 5.1). This makes holonomy computable and interpretable, rather than an abstract loop product.
- **(B) Shearing implies unavoidable mismatch.** The shearing score  $D_{\text{shear}}(u, v)$  lower-bounds a concrete transfer mismatch energy on overlap data (Theorem 4.2). This turns shearing into an obstruction with operational meaning.
- **(C) Certified jamming forces interference.** A non-vacuous lower bound certifies forced interference on a consequential subset of atoms (Theorem 6.2). We evaluate not merely correctness, but also non-vacuity (coverage), and robustness across seeds and hyperparameters.
- **(D) Estimator stability.** Bootstrap and sample-size curves establish that  $D_{\text{shear}}$  and  $D_{\text{hol}}$  are stable measurements under finite overlap sampling, especially on well-conditioned persistent subsystems (Section 7).

## 1.2 Significance and impact

Most mechanistic interpretability work implicitly assumes that a single, globally consistent feature dictionary can describe a layer across diverse contexts. Our results show that this premise can fail in structured, measurable ways even for a frozen model, and we propose a concrete alternative: interpretability as an *atlas construction problem* with explicit local-to-global obstructions. The central impact is methodological: we turn context dependence from an informal caveat into a set of *computable, falsifiable diagnostics* that decompose global failure into three distinct mechanisms—local overload (jamming), cross-chart incompatibility (proxy shearing), and intrinsically path-dependent transport (holonomy).

Concretely, Result A provides a constructive gauge computation that reduces holonomy from an abstract loop statistic to a directly checkable quantity: after spanning-tree gauge fixing, chord residuals coincide with fundamental-cycle holonomy, and the identity checks hold to numerical precision. Result B connects proxy disagreement to operational consequences by lower-bounding a realised transfer-mismatch energy, making large shearing edges interpretable as unavoidable cross-context mismatch *with respect to a fixed correspondence proxy*. Result C shows that interference need not remain qualitative: we obtain *non-vacuous* certified lower bounds on consequential subsets with high coverage and zero violations across random seeds and hyperparameters. Finally, Result D establishes that the proposed measurements are not fragile artefacts of overlap sampling: bootstrap and sample-size experiments show concentration with increasing overlap size and improved stability under conditioning-based persistence filtering.

Taken together, the framework supplies evaluation primitives for *when* and *why* global interpretability breaks, enabling atlas-level summaries that are reproducible, stability-tested, and comparable across subsystems, rather than anecdotal case studies.

## 1.3 Related work

Superposition toy models and monosemantic feature extraction motivate our focus on interference and overcomplete features Elhage et al. (2022); Bricken et al. (2023); Templeton et al. (2024). Our use of Fisher/Gauss–Newton geometry follows classical information geometry and second-order optimisation literature Amari (2016); Martens & Grosse (2015). The atlas perspective is naturally expressed using cellular sheaves, which provide a principled language for local-to-global structure over combinatorial bases Curry (2014); Hansen & Ghrist (2019). Neural message-passing models have recently incorporated sheaf-theoretic structure explicitly, providing complementary perspectives on local-to-global consistency and transport

constraints Bodnar et al. (2022). In particular, cooperative sheaf constructions study how multiple local predictors can be coupled via sheaf constraints, offering a modern ML analogue of atlas-style consistency conditions Ribeiro et al. (2025). Our gauge/holonomy viewpoint is aligned with group synchronisation on graphs Singer (2011), but differs in that the underlying objects are derived from learned transports and correspondence proxies rather than direct measurements of group elements. Recent work has proposed *representation holonomy* as a gauge-invariant statistic for path dependence in learned representations, with estimators based on (whitened) local Procrustes alignment around loops in input space Sevetlidis & Pavlidis (2026). Our setting differs in both object and goal: we build an *atlas over context clusters* (a discrete context complex) and study transports/defects on the resulting chart graph rather than input-space neighborhoods. Moreover, we connect holonomy to a constructive *spanning-tree gauge computation* that makes fundamental-cycle holonomy directly computable from chord defects (Theorem 5.1), and we complement holonomy with two additional, operational obstructions—proxy shearing (Theorem 4.2) and certified jamming/interference (Theorem 6.2).

**Scope.** Sevetlidis & Pavlidis (2026) introduces holonomy as a representation-level diagnostic on input-space loops, whereas we use holonomy as one component of a broader atlas-based interpretability objective on a context-cluster graph. Accordingly, our shearing and jamming analyses are intentionally proxy- and model-class-specific (see Limitations), and our contribution is the combination of (i) an explicit chart-graph construction, (ii) a gauge-fixing computation that reduces holonomy to chord defects (Theorem 5.1), and (iii) complementary certified and stable diagnostics for local interference and cross-chart mismatch (Theorems 4.2–6.2, Result D).

## 2 Setup: context complex, local charts, transports

### 2.1 Activations and clustering

Fix a frozen model and layer  $\ell$  with activation space  $\mathbb{R}^d$ . From a token dataset  $\mathcal{X}$ , extract token-level activations  $\{x_t\}_{t=1}^N \subset \mathbb{R}^d$ . Cluster the activations into  $C$  clusters  $\{\mathcal{D}_c\}_{c=1}^C$  McQueen (1967). Clusters act as *local charts*.

### 2.2 Stratified context complex

**Definition 2.1** (Stratified context complex). *Let  $\mathcal{K}$  be a finite simplicial complex (in practice, we use its 1-skeleton  $G = (V, E)$ ) whose vertices index context clusters. Assume a stratification  $\mathcal{K} = \bigsqcup_{s \in \mathcal{S}} \mathcal{K}_s$  where each stratum is approximately homogeneous with respect to a context class (e.g. prose vs code).*

Stratification is not required for the definitions below, but is used to interpret which transitions induce large shearing or holonomy.

### 2.3 Local feature spaces and frames

**Definition 2.2** (Local frame). *Let  $U \subseteq \mathbb{R}^d$  be finite-dimensional. A set  $\{e_i\}_{i=1}^m \subset U$  is a frame if it spans  $U$  Christensen et al. (2003). It is overcomplete if  $m > \dim U$ .*

In experiments we use two chart representations: (i) an orthonormal  $k$ -dimensional PCA chart basis (for transports/holonomy), and (ii) a local overcomplete dictionary learned by sparse coding (for jamming/interference).

### 2.4 Rectangular partial transports

**Definition 2.3** (Rectangular partial transport). *For each oriented edge  $u \rightarrow v$  in the chart graph, define*

$$T_{vu} : F_u \rightarrow F_v, \quad T_{vu} \in \mathbb{R}^{m_v \times m_u}.$$

Rank variation accommodates partial persistence, merging, splitting, and birth/death of features across contexts.

### 3 Local information geometry and Fisher-weighted interference

#### 3.1 Local Fisher/Gauss–Newton metric

Let  $p_\theta(y | x)$  be the model output distribution. In local coordinates  $z = z^{(c)}(x)$  define

$$G^{(c)} := \mathbb{E}_{x \sim \mathcal{D}_c} [g_z(x) g_z(x)^\top] \in \mathbb{R}^{m_c \times m_c}, \quad g_z(x) := D_c g_x(x), \quad g_x(x) := \nabla_{x_\ell} \ell(x) \in \mathbb{R}^d, \quad (1)$$

where  $\ell(x)$  is the next-token negative log-likelihood of the frozen model,  $x_\ell$  denotes the layer- $\ell$  activation vector, and  $D_c \in \mathbb{R}^{m_c \times d}$  is the learned per-chart *encoder* mapping activations to code space (we write codes as  $z = D_c x_\ell$ ). Equivalently, if  $E_c \in \mathbb{R}^{d \times m_c}$  denotes a decoder dictionary with column atoms, then  $D_c$  is the corresponding encoder used for code-space gradients. In experiments we compute  $g_x$  by backpropagating  $\ell$ , map to code-space gradients  $g_z = D_c g_x$ , and estimate  $G^{(c)}$  by the empirical outer product

$$\widehat{G}^{(c)} = \frac{1}{n} \sum_{i=1}^n g_{z,i} g_{z,i}^\top.$$

**Proposition 3.1** (PSD).  $G^{(c)}$  is symmetric positive semidefinite.

*Proof.*  $G^{(c)} = \mathbb{E}[g_z g_z^\top]$  with  $g_z = D_c \nabla_{x_\ell} \ell(x)$ , hence  $a^\top G^{(c)} a = \mathbb{E}[(a^\top g_z)^2] \geq 0$ .  $\square$

#### 3.2 Harm matrix

Raw off-diagonal Fisher entries can be negative; using them directly would reward certain overlaps. We instead construct nonnegative interaction weights.

**Definition 3.2** (Harm matrix). Fix  $\tau > 0$ . Define the diagonally normalised Fisher

$$\widetilde{G}^{(c)} := (\text{diag}(G^{(c)}) + \tau I)^{-1/2} G^{(c)} (\text{diag}(G^{(c)}) + \tau I)^{-1/2}.$$

Define  $W^{(c)} \in \mathbb{R}_+^{m_c \times m_c}$  with zero diagonal by

$$W_{ij}^{(c)} := \begin{cases} \eta\left(\left|\widetilde{G}_{ij}^{(c)}\right|\right), & i \neq j, \\ 0, & i = j, \end{cases}$$

with monotone  $\eta$  (canonical:  $\eta(t) = t$ ).

#### 3.3 Frame geometry and interference energy

Let  $E_c \in \mathbb{R}^{d \times m_c}$  be a decoder/dictionary matrix with columns  $e_i^{(c)}$ . Let  $\widehat{E}_c = E_c (D_c^{(E)})^{-1/2}$  where  $D_c^{(E)} = \text{diag}(\|e_1\|^2, \dots, \|e_{m_c}\|^2)$ . Define  $K^{(c)} = \widehat{E}_c^\top \widehat{E}_c$ .

**Definition 3.3** (Local Fisher-weighted interference energy).

$$\mathcal{E}(c) := \sum_{i \neq j} W_{ij}^{(c)} (K_{ij}^{(c)})^2 = \left\| \left( W^{(c)} \right)^{\odot \frac{1}{2}} \odot (K^{(c)} - I) \right\|_F^2.$$

**Proposition 3.4** (Nonnegativity and zero set).  $\mathcal{E}(c) \geq 0$ . Moreover,  $\mathcal{E}(c) = 0$  iff  $K_{ij}^{(c)} = 0$  for all  $i \neq j$  with  $W_{ij}^{(c)} > 0$ .

*Proof.* Each summand is nonnegative; the sum is zero iff each summand is zero.  $\square$

### 3.4 Effective rank and the jamming index

**Definition 3.5** (Effective rank). For PSD  $G \neq 0$ ,

$$R_{\text{eff}}(G) := \frac{\text{Tr}(G)^2}{\text{Tr}(G^2)}.$$

**Proposition 3.6** (Basic properties).  $R_{\text{eff}}(\alpha G) = R_{\text{eff}}(G)$  for  $\alpha > 0$ , and  $1 \leq R_{\text{eff}}(G) \leq \text{rank}(G)$ .

**Definition 3.7** (Participation-ratio active count). For codes  $z \in \mathbb{R}^{m^c}$  define  $k_{\text{PR}}(z) = \|z\|_1^2 / \|z\|_2^2$  (with  $k_{\text{PR}}(0) = 0$ ) and

$$k_{\text{active}}(c) := \mathbb{E}[k_{\text{PR}}(z^{(c)}(x))].$$

**Definition 3.8** (Local jamming index).

$$J(c) := \frac{k_{\text{active}}(c)}{R_{\text{eff}}(G^{(c)})}.$$

### 3.5 Welch-type baseline lower bound

**Proposition 3.9** (Weighted Welch-type lower bound). Let  $A$  index  $k$  unit vectors lying in an  $r$ -dimensional subspace. If  $(W_A)_{ij} \geq w_{\min} > 0$  for all  $i \neq j$  in  $A$ , then

$$\mathcal{E}_A(c) := \sum_{i \neq j \in A} W_{ij}^{(c)} (K_{ij}^{(c)})^2 \geq w_{\min} \left( \frac{k^2}{r} - k \right).$$

*Proof.* Standard Welch bound Welch (1974):  $\text{Tr}(G_A^2) \geq (\text{Tr} G_A)^2 / \text{rank}(G_A) \geq k^2 / r$  implies  $\sum_{i \neq j} \langle e_i, e_j \rangle^2 \geq k^2 / r - k$ . Multiply by  $w_{\min}$ .  $\square$

This proposition is mathematically correct but often practically weak because  $w_{\min}$  across all pairs can be very small. Theorem 6.2 resolves this by certifying a consequential subset with a nontrivial uniform weight floor.

## 4 Proxy shearing and Theorem B

### 4.1 Geometric transport and correspondence proxy

Let  $(u, v)$  be a graph edge with overlap samples  $X_{uv}$ . Work on a shared  $k$ -dimensional support (e.g. chart PCA subspace). Let  $Z_u, Z_v \in \mathbb{R}^{k \times n}$  be overlap coordinates. Estimate a transport  $\hat{T}_{vu}$  and define the orthogonal polar factor  $Q_{vu} = \text{polar}(\hat{T}_{vu}) \in O(k)$  Higham (1986); Schönemann (1966).

Let  $\hat{P}_{vu} \in O(k)$  be a fixed, reproducible correspondence proxy on the same support. In our experiments,  $\hat{P}_{vu}$  is constructed as a Procrustes-style correspondence proxy from the fitted PCA chart bases (Section 4.1), and all reported  $D_{\text{shear}}$ ,  $g_{vu}$ , and holonomy values use this choice. The shearing score measures disagreement between the geometry-derived transport and the correspondence proxy.

**Concrete definition of  $\hat{P}_{vu}$  (default proxy).** To make  $D_{\text{shear}}$  reproducible, we fix  $\hat{P}_{vu}$  as a Procrustes-style correspondence proxy derived from the local PCA chart bases. Let  $B_u, B_v \in \mathbb{R}^{d \times k}$  denote the orthonormal PCA bases fitted per chart (Algorithm 1). Define the  $k \times k$  basis overlap matrix

$$S_{vu} := B_v^\top B_u.$$

We then set the proxy to be the orthogonal polar factor of  $S_{vu}$ :

$$\hat{P}_{vu} := \text{polar}(S_{vu}) \in O(k),$$

i.e. if  $S_{vu} = U\Sigma V^\top$  is an SVD, then  $\text{polar}(S_{vu}) = UV^\top$  Higham (1986); Schönemann (1966). This proxy is deterministic given the fitted chart bases and does not require an additional matching procedure on overlap statistics.

**Definition 4.1** (Normalised shearing).

$$D_{\text{shear}}(u, v) := \frac{\|Q_{vu} - \widehat{P}_{vu}\|_F}{2\sqrt{k}} \in [0, 1].$$

## 4.2 Theorem B: shearing lower-bounds transfer mismatch

Let  $z_u$  denote overlap codes in chart  $u$ , with covariance  $\Sigma_u = \mathbb{E}[z_u z_u^\top] \succeq 0$ . Define the transfer mismatch energy

$$\Delta_{uv} := \mathbb{E} \|(Q_{vu} - \widehat{P}_{vu})z_u\|_2^2.$$

**Theorem 4.2** (Shearing lower-bounds transfer mismatch). *Let  $A_{vu} := Q_{vu} - \widehat{P}_{vu}$  and  $\Sigma_u \succeq 0$ . Then*

$$\Delta_{uv} = \text{Tr}(A_{vu} \Sigma_u A_{vu}^\top) \geq \lambda_{\min}(\Sigma_u) \|A_{vu}\|_F^2 = 4k \lambda_{\min}(\Sigma_u) D_{\text{shear}}(u, v)^2.$$

*Proof.* Since  $\Sigma_u \succeq \lambda_{\min}(\Sigma_u)I$  on the shared support,  $\text{Tr}(A \Sigma_u A^\top) \geq \lambda_{\min}(\Sigma_u) \text{Tr}(A A^\top) = \lambda_{\min}(\Sigma_u) \|A\|_F^2$ . Substitute  $\|A\|_F = 2\sqrt{k} D_{\text{shear}}$ .  $\square$

All ‘‘mismatch’’ statements here are with respect to the fixed proxy  $\widehat{P}_{vu}$  defined above (not an absolute notion of semantics). The empirical section will report both  $\widehat{\Delta}_{uv}$  and the lower bound  $\widehat{\text{LB}}_{uv} := \lambda_{\min}(\widehat{\Sigma}_u) \|A_{vu}\|_F^2$ , and will quantify the *slack*  $\widehat{\Delta}_{uv} / \widehat{\text{LB}}_{uv}$ . Large slack indicates conservativeness caused by small  $\lambda_{\min}(\widehat{\Sigma}_u)$  (anisotropic overlap excitation), not a failure of the theorem.

## 5 Gauge structure, holonomy, and Theorem A

### 5.1 Edge defects, gauge action, holonomy

Assume a connected graph  $G = (V, E)$  and orthogonal edge defects  $g_{vu} \in O(k)$  on oriented edges. A gauge is an assignment  $U_c \in O(k)$  at each vertex, acting by

$$g_{vu} \mapsto g'_{vu} := U_v g_{vu} U_u^\top.$$

For a directed loop  $\gamma : c_0 \rightarrow \cdots \rightarrow c_L = c_0$  define holonomy

$$h_\gamma := g_{c_0 c_{L-1}} \cdots g_{c_1 c_0} \in O(k).$$

Under gauge,  $h_\gamma$  transforms by conjugation at  $c_0$ , hence  $\|h_\gamma - I\|_F$  is gauge invariant. We use the normalised defect

$$D_{\text{hol}}(\gamma) := \frac{\|h_\gamma - I\|_F}{\sqrt{2k}} \in [0, 1].$$

### 5.2 Theorem A: spanning-tree gauge identity

**Theorem 5.1** (Spanning-tree gauge and fundamental-cycle holonomy). *Let  $G = (V, E)$  be connected and  $T \subseteq G$  a spanning tree rooted at  $r$  with parent map  $\pi(v)$ . Define*

$$U_r := I, \quad U_v := U_{\pi(v)} g_{\pi(v), v} \quad (v \neq r).$$

*Then:*

(i) *For each tree edge  $\pi(v) \rightarrow v$ ,  $g'_{v, \pi(v)} = I$ .*

(ii) *For each chord  $e = \{u, v\} \notin T$ , the gauged chord defect equals the holonomy of the fundamental cycle  $\gamma_e$ :*

$$g'_{vu} = h_{\gamma_e}.$$

*Proof.* Tree edges:  $g'_{v,\pi(v)} = (U_{\pi(v)}g_{\pi(v),v})g_{v,\pi(v)}U_{\pi(v)}^\top = U_{\pi(v)}IU_{\pi(v)}^\top = I$  since  $g_{\pi(v),v} = g_{v,\pi(v)}^{-1}$ .

Chord edges: write  $g'_{vu} = U_v g_{vu} U_u^\top$  and expand  $U_v$  and  $U_u$  as products along tree paths from  $r$ . Common path factors cancel (telescoping), leaving the ordered product along the unique tree path from  $u$  to  $v$  and the chord  $v \rightarrow u$ , which is precisely the loop product defining  $h_{\gamma_e}$ .  $\square$

### 5.3 Holonomy obstruction criterion

**Theorem 5.2** (Holonomy obstruction). *If there exists a gauge such that  $g'_{vu} = I$  for all edges in a connected subgraph, then  $h_\gamma = I$  for every loop  $\gamma$  in that subgraph. Equivalently, if some loop has  $h_\gamma \neq I$ , then no globally connection-compatible trivialisation exists on that subsystem.*

*Proof.* If every edge defect is identity in a gauge, every loop product is a product of identities.  $\square$

Theorem 5.1 supplies a computational strategy: choose a spanning tree in the LCC, gauge-fix it, then compute holonomy only on chords (each chord generates one fundamental cycle). The experiments will show that (i) tree residuals are numerically near zero, and (ii) chord residuals match holonomy to numerical precision, which is the quantitative validation of Theorem 5.1 in an LLM setting.

## 6 Certified jamming/interference: Theorem C

### 6.1 Projected setting and consequential subsets

Fix a chart  $c$ . Let  $D_c \in \mathbb{R}^{m \times d}$  be a dictionary with unit atoms  $\widehat{D}_{c,i}$ . Let  $W^{(c)}$  be the harm matrix in code space. Let  $r = \lceil R_{\text{eff}}(G^{(c)}) \rceil$  and let  $B_r \in \mathbb{R}^{d \times r}$  be the top- $r$  PCA basis of chart activations. Project atoms to  $\mathbb{R}^r$  by

$$a_i := \widehat{D}_{c,i} B_r, \quad \widehat{a}_i := a_i / \|a_i\|_2,$$

and define projected Gram  $K_{ij}^{(r)} := \langle \widehat{a}_i, \widehat{a}_j \rangle$  with  $K_{ii}^{(r)} = 0$ .

**Definition 6.1** ( $\tau$ -consequential subset). *A subset  $A \subseteq \{1, \dots, m\}$  is  $\tau_\star$ -consequential if  $W_{ij}^{(c)} \geq \tau_\star$  for all distinct  $i, j \in A$ .*

### 6.2 Theorem C

**Theorem 6.2** (Certified interference on a consequential subset). *Let  $A$  be  $\tau_\star$ -consequential and  $k := |A|$ . Then*

$$\mathcal{E}_A^{(r)}(c) := \sum_{i \neq j \in A} W_{ij}^{(c)} (K_{ij}^{(r)})^2 \geq \widehat{\text{LB}}(c) := \tau_\star \left( \frac{k^2}{r} - k \right)_+.$$

*Proof.* The vectors  $\widehat{a}_i$  lie in  $\mathbb{R}^r$  and are unit norm. Let  $G_A$  be their Gram matrix. Then  $\text{rank}(G_A) \leq r$  and  $\text{Tr}(G_A) = k$ . By Cauchy–Schwarz on eigenvalues,  $\text{Tr}(G_A^2) \geq \text{Tr}(G_A)^2 / \text{rank}(G_A) \geq k^2 / r$ . Hence  $\sum_{i \neq j \in A} \langle \widehat{a}_i, \widehat{a}_j \rangle^2 = \text{Tr}(G_A^2) - k \geq k^2 / r - k$ . Since  $W_{ij}^{(c)} \geq \tau_\star$  on  $A$ , the stated bound follows.  $\square$

The experimental section will report (i) coverage: how many charts achieve  $\widehat{\text{LB}}(c) > 0$ , (ii) correctness: slack  $\mathcal{E}_A^{(r)}(c) / \widehat{\text{LB}}(c) \geq 1$  with zero violations, and (iii) robustness across seeds and  $(m, \alpha)$ .

## 7 Stability and concentration: Result D

### 7.1 Why conditioning matters: polar factor perturbation

**Lemma 7.1** (Polar factor stability). *Let  $T$  be nonsingular with  $\sigma_{\min}(T) \geq s > 0$  and  $\|\Delta T\|_2 \leq s/2$ . Then*

$$\|\text{polar}(T + \Delta T) - \text{polar}(T)\|_F \leq C \frac{\|\Delta T\|_F}{s}$$

for a universal constant  $C$  Higham (1986).

## 7.2 Loop accumulation bound

**Lemma 7.2** (Loop product telescoping bound). For  $g_i, \tilde{g}_i \in O(k)$ ,

$$\left\| \prod_{i=1}^L g_i - \prod_{i=1}^L \tilde{g}_i \right\|_F \leq \sum_{i=1}^L \|g_i - \tilde{g}_i\|_F.$$

*Proof.* Expand the difference as a telescoping sum. Orthogonal left/right multiplication preserves Frobenius norm.  $\square$

Lemmas 7.1 and 7.2 predict two testable behaviours: (i) edge diagnostics based on polar factors are less variable when  $\sigma_{\min}(T_{vu})$  is bounded away from 0, and (ii) loop diagnostics are stable when edge diagnostics are stable, with variability accumulating with loop length. The experiments quantify these predictions with global bootstrap summaries and within-edge/within-loop sample-size curves.

## 8 Atlas Method (pipeline)

This section states the pipeline used in experiments and clarifies which stage produces which reported numbers. It is included because results A–D depend on multiple intermediate objects (clusters, overlaps, transports, proxies, loops), and reproducibility requires an explicit map from objects to measurements.

### 8.1 Pipeline summary

---

**Algorithm 1** Atlas Method (post-hoc cartography)

---

**Require:** Frozen model  $\theta$ , layer  $\ell$ , dataset  $\mathcal{X}$ , clusters  $C$ , support dimension  $k$

**Ensure:** Graph  $G$ , edge defects  $g_{vu}$ , shearing  $D_{\text{shear}}$ , holonomy  $D_{\text{hol}}$ , jamming diagnostics

- 1: Extract token-level activations  $\{x_t\}_{t=1}^N \subset \mathbb{R}^d$  at layer  $\ell$  (optionally subsampling tokens for storage/compute).
  - 2: Cluster activations into  $C$  charts; build centroid  $k$ -NN graph  $G = (V, E)$ .
  - 3: For each chart  $c$ : fit PCA basis  $B_c \in \mathbb{R}^{d \times k}$  Jolliffe (2005).
  - 4: For jamming/interference (Result C): collect per-chart samples  $(x_\ell, g_x)$  with  $g_x = \nabla_{x_\ell} \ell(x)$  (next-token NLL), fit an overcomplete dictionary  $D_c$  and sparse codes  $z$ , and form  $\widehat{G}^{(c)} = \frac{1}{n} \sum_i (D_c g_{x,i})(D_c g_{x,i})^\top$ .
  - 5: For each edge  $(u, v)$ : build overlap set  $X_{uv}$ ; compute overlap coordinates  $Z_u = B_u^\top X_{uv}$ ,  $Z_v = B_v^\top X_{uv}$ .
  - 6: Estimate  $\widehat{T}_{vu}$  by ridge regression Hoerl & Kennard (1970):  $\widehat{T}_{vu} := Z_v Z_u^\top (Z_u Z_u^\top + \lambda I)^{-1}$ ; compute  $Q_{vu} := \text{polar}(\widehat{T}_{vu})$ .
  - 7: Construct the correspondence proxy  $\widehat{P}_{vu} := \text{polar}(B_v^\top B_u)$  on the shared support (Section 4.1), and define the edge defect  $g_{vu} = \widehat{P}_{vu}^\top Q_{vu}$ .
  - 8: Compute  $D_{\text{shear}}(u, v)$ .
  - 9: Choose spanning tree in LCC; compute chord holonomies and  $D_{\text{hol}}$  via Theorem 5.1.
  - 10: (Optional) Filter edges by  $\sigma_{\min}(\widehat{T}_{vu}) \geq s_{\min}$  to form persistent subsystem and repeat steps 6–7.
- 

### 8.2 Interpretation of the persistence filter

Filtering edges by  $\sigma_{\min}(\widehat{T}_{vu}) \geq s_{\min}$  operationalises the conditioning requirement suggested by Lemma 7.1. This filter changes *both* numerical stability and the graph topology: it can reduce the number of cycles available for holonomy computation. The experiments report this tradeoff explicitly in Table 2.

---

## 9 Experiments

### 9.1 Experimental setup

We used `meta-llama/Llama-3.2-3B-Instruct` and extracted activations at layer  $\ell = 16$  with  $d = 3072$  Meta (2024). We used three data sources to obtain heterogeneous contexts: WikiText-103 (raw) for prose, a C4-derived English web-text subset (from `PrimeIntellect/c4-tiny` when available, otherwise streamed from `allenai/c4`), and code from `bigcode/the-stack-smol` Merity et al. (2016); Raffel et al. (2020); Kocetkov et al. (2022). We extracted and stored  $N \approx 2 \times 10^5$  token activations *after subsampling tokens* (every 8 tokens per sequence by default), clustered these activations into  $C = 128$  clusters, and built a centroid  $k$ -NN graph. For transports and holonomy we used a shared chart support dimension  $k = 32$ .

Overlap sets  $X_{uv}$  were constructed by a Voronoi rule: an activation belongs to  $X_{uv}$  if its nearest and second-nearest centroids are  $\{u, v\}$ . In implementation, we compute nearest and second-nearest centroids from the fitted centroid set for each activation and form overlaps accordingly. This concentrates overlap data near the boundary between clusters, which empirically improves transport fit stability relative to using all points in both clusters.

### 9.2 A: spanning-tree gauge identity and persistence tradeoff

Result A makes two claims that are checkable numerically: (i) after spanning-tree gauge fixing, tree-edge residuals are (numerically) zero, and (ii) for each chord, the chord residual equals the holonomy of the associated fundamental cycle.

**Quantitative identity check (tree residuals and chord/holonomy agreement).** For each oriented edge we formed  $g_{vu} = \widehat{P}_{vu}^\top Q_{vu} \in O(k)$ . We built a spanning tree on the LCC and constructed the spanning-tree gauge ( $U_c$ ) from Theorem 5.1. We then measured:

$$r_{\text{tree}} := \|U_v g_{vu} U_u^\top - I\|_F \quad \text{on tree edges}, \quad r_{\text{chord}} := \|U_v g_{vu} U_u^\top - I\|_F \quad \text{on chords}.$$

By Theorem 5.1, chord residuals equal fundamental-cycle holonomy defects  $\|h_{\gamma_e} - I\|_F$ . In our runs the mean absolute difference between chord residual and holonomy defect was  $\sim 10^{-6}$ , i.e. numerical precision; tree residuals were  $\sim 10^{-5}$  due to floating-point error and orthogonal projection.

Table 1 reports the identity-check statistics for baseline ( $s_{\min} = 0$ ) and persistent ( $s_{\min} = 0.015$ ) subsystems. The key interpretation is: *the tree residuals are near zero, while chord residuals are large and match holonomy*. This directly supports the claim that holonomy is not a coordinate artefact: it is exactly what remains after maximal gauge fixing.

Table 1: Result A identity checks on the LCC ( $k = 32$ ). Tree residuals quantify successful gauge fixing on the spanning tree. Chord residuals coincide with fundamental-cycle holonomy as predicted by Theorem 5.1.

Subsystem	Tree residual mean	Tree residual max	Chord/hol mean $\ h - I\ _F$	Chord/hol max $\ h - I\ _F$
Baseline ( $s_{\min} = 0$ )	$1.6003 \times 10^{-5}$	$2.3228 \times 10^{-5}$	4.4330	6.7364
Persistent ( $s_{\min} = 0.015$ )	$1.9701 \times 10^{-5}$	$3.1521 \times 10^{-5}$	4.0650	6.3957

**Persistence sweep (conditioning vs connectivity vs holonomy).** The persistence threshold  $s_{\min}$  filters edges by  $\sigma_{\min}(\widehat{T}_{vu}) \geq s_{\min}$ . This improves conditioning and, empirically, reduces holonomy magnitudes; but it also removes edges and can collapse cycles. Table 2 quantifies this tradeoff.

The column  $E_{LCC}$  is the number of edges remaining in the LCC after filtering; it measures how much transition information remains connected. The column #chords is the number of non-tree edges; it is the number of independent fundamental cycles available for holonomy computation on that LCC. The last two columns report mean and max normalised holonomy defect  $D_{\text{hol}} = \|h - I\|_F / \sqrt{2k}$ . The numerical pattern shows:

- As  $s_{\min}$  increases, mean  $D_{\text{hol}}$  decreases from 0.554 at  $s_{\min} = 0$  to 0.456 at  $s_{\min} = 0.02$ , suggesting that poorly conditioned edges inflate apparent curvature.
- The number of available cycles decreases sharply (84 chords at baseline to 17 at  $s_{\min} = 0.02$ ), meaning aggressive filtering can make holonomy estimates less representative simply because fewer loops remain.

Table 2: Persistence sweep ( $k = 32$ ). Increasing  $s_{\min}$  improves conditioning but reduces connectivity and cycle availability. The reported  $D_{\text{hol}}$  values are computed on fundamental cycles induced by chords in the LCC.

$s_{\min}$	$E_{\text{LCC}}$	LCC size	#chords	mean $D_{\text{hol}}$	max $D_{\text{hol}}$
0.0000	173	90	84	0.554	0.842
0.0100	129	84	46	0.517	0.799
0.0125	106	73	34	0.517	0.799
0.0150	90	62	29	0.508	0.799
0.0200	75	59	17	0.456	0.789

**Distributional view of holonomy (figure interpretation).** Figure 1 complements Table 2 by showing the full distribution of  $D_{\text{hol}}$  values for baseline and persistent subsystems. The histogram shows how mass shifts; the ECDF highlights tail behaviour (high-holonomy loops). In this run the persistent distribution is shifted toward smaller values, but retains a substantial upper tail, indicating that improved conditioning does not eliminate genuine path dependence.

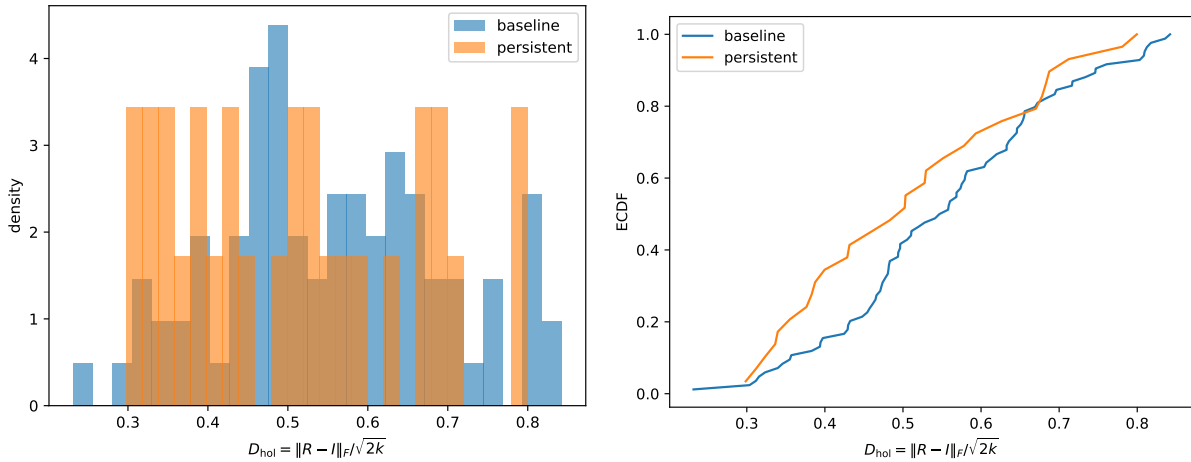


Figure 1: Holonomy defect distributions (normalised) comparing baseline ( $s_{\min} = 0$ ) and persistent ( $s_{\min} = 0.015$ ) subsystems.

### 9.3 B: empirical validation of Theorem B (shearing bound)

Theorem 4.2 is a deterministic inequality. Empirically, we evaluate its instantiated quantities on each edge:

$$\widehat{\Delta}_{uv} = \frac{1}{n} \|(Q_{vu} - \widehat{P}_{vu})Z_u\|_F^2, \quad \widehat{\text{LB}}_{uv} = \lambda_{\min}(\widehat{\Sigma}_u) \|Q_{vu} - \widehat{P}_{vu}\|_F^2,$$

where  $\widehat{\Sigma}_u = \frac{1}{n} Z_u Z_u^\top$ . We report slack  $\widehat{\Delta}_{uv} / \widehat{\text{LB}}_{uv}$  (with numerical stabilisation). Slack should satisfy  $\widehat{\Delta}_{uv} / \widehat{\text{LB}}_{uv} \geq 1$  up to numerical error when  $\widehat{\text{LB}}_{uv} > 0$ ; values much larger than 1 indicate that the bound is conservative.

**Edge-level distributions (numbers and meaning).** Table 3 summarises two aspects of Result B: (i) the distribution of  $D_{\text{shear}}$  (how large the geometric/semantic mismatch is), and (ii) the distribution of slack (how conservative the theoretical bound is on real overlap covariance). For the baseline subsystem, mean  $D_{\text{shear}}$  is 0.2015 with max 0.3743. For the persistent subsystem, mean  $D_{\text{shear}}$  is 0.1910 with max 0.3730. This indicates that conditioning-based filtering slightly reduces average mismatch, but does not remove large-shearing edges. Slack medians are around 7.8, meaning  $\widehat{\Delta}_{uv}$  is typically an order of magnitude larger than the eigenvalue-based lower bound; this is expected when  $\lambda_{\min}(\widehat{\Sigma}_u)$  is small.

Table 3: Result B summary statistics for shearing and slack (normalised) computed over all retained edges in the subsystem. Slack is  $\widehat{\Delta}_{uv}/\widehat{\text{LB}}_{uv}$ ; values  $> 1$  confirm the bound (up to numerical error), and large values quantify conservativeness due to small  $\lambda_{\min}(\widehat{\Sigma}_u)$ .

Subsystem	$n_{\text{edges}}$	$D_{\text{min}}$	$D_{\text{med}}$	$D_{\text{mean}}$	$D_{\text{max}}$	slack <sub>min</sub>	slack <sub>med</sub>	slack <sub>max</sub>
Baseline	173	0.0354	0.2080	0.2015	0.3743	2.314	7.802	399.525
Persistent	90	0.0637	0.1966	0.1910	0.3730	2.565	7.837	399.525

**Figure interpretation (why each panel exists).** Figures 2 and 3 each contain three panels:

1.  $\widehat{\Delta}$  vs  $\widehat{\text{LB}}$ : points above the diagonal confirm the inequality edge-by-edge.
2.  $\widehat{\Delta}$  vs  $D_{\text{shear}}$ : demonstrates that larger mismatch scores correspond to larger realised transfer mismatch energies.
3. *Slack histogram*: quantifies how conservative the bound is; heavy tails arise when some edges have extremely small  $\lambda_{\min}(\widehat{\Sigma}_u)$ .

In combination, these panels demonstrate (i) correctness, (ii) monotone usefulness, and (iii) the bound’s tightness regime. For visualisation we exclude edges with near-zero  $\lambda_{\min}(\widehat{\Sigma}_u)$  (e.g.  $\lambda_{\min} < 10^{-6}$ ), since the bound becomes numerically trivial and slack is dominated by stabilisation constants.

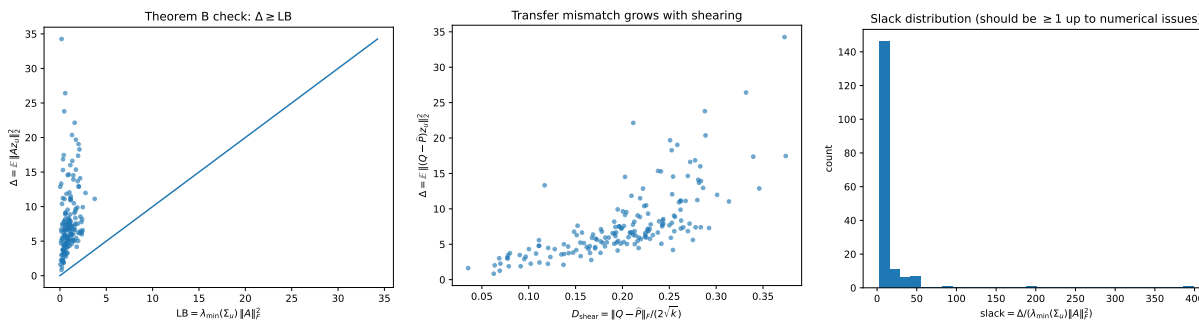


Figure 2: Baseline subsystem: (left)  $\widehat{\Delta}_{uv}$  vs lower bound  $\widehat{\text{LB}}_{uv}$  (points above diagonal), (middle)  $\widehat{\Delta}_{uv}$  vs  $D_{\text{shear}}(u, v)$ , (right) slack distribution.

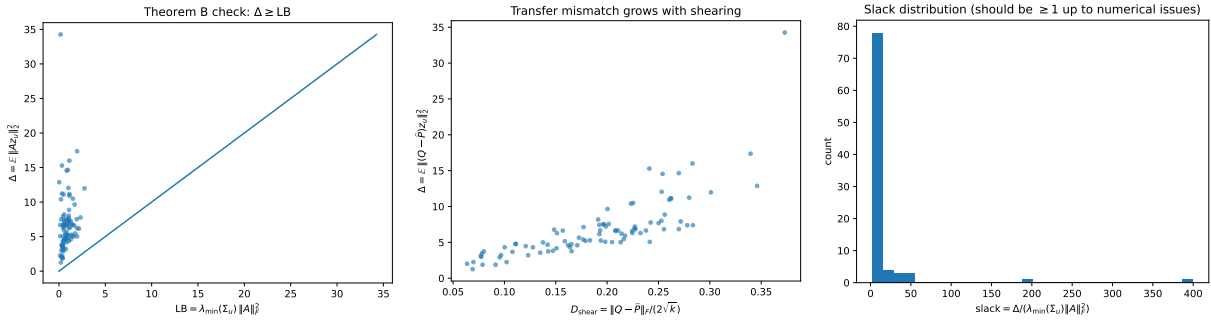


Figure 3: Persistent subsystem ( $s_{\min} = 0.015$ ): the same diagnostics as Figure 2.

### 9.4 C: certified jamming/interference (coverage, correctness, robustness)

Theorem 6.2 is a deterministic certificate once the consequential subset  $A$  and threshold  $\tau_*$  are fixed. Empirically, the key scientific questions are:

1. **Non-vacuity (coverage):** how often does the procedure find  $A$  with  $\widehat{\text{LB}}(c) > 0$ ?
2. **Correctness:** are there any violations of  $\mathcal{E}_A^{(r)}(c) \geq \widehat{\text{LB}}(c)$  (slack  $< 1$ )?
3. **Robustness:** are coverage/correctness stable across random seeds and dictionary hyperparameters?

**What the reported quantities mean.** Cert. charts is the number of charts (out of 40 analysed) with  $\widehat{\text{LB}}(c) > 0$ ; this is the non-vacuity measure. Slack is  $\mathcal{E}_A^{(r)}(c) / \widehat{\text{LB}}(c)$  on certified charts; slack must be  $\geq 1$ . Slack minimum therefore acts as a stringent correctness check.  $\text{Corr}(J, \mathcal{E}^{(r)})$  and  $\text{Corr}(J, \mathcal{E}_A^{(r)})$  measure whether the diagnostic  $J(c)$  tracks observed interference energies; these correlations are empirical and not part of the certificate.

**Seed stability.** Table 4 shows that for  $m = 256, \alpha = 1.0$  the certification rate is 0.85–0.875 across seeds, and slack minima remain comfortably above 1 (no violations). These numbers mean that the certificate is not a rare event: most charts admit a nontrivial lower bound, and the algorithmic construction is not sensitive to random initialisation.

Table 4: Seed stability for Result C (fixed  $m = 256, \alpha = 1.0$ ; 40 charts). Cert. rate measures non-vacuity. Slack min  $> 1$  indicates zero violations. Correlations quantify the empirical association between jamming and interference.

Seed	Cert. charts	Cert. rate	Slack median	Slack min	$\text{Corr}(J, \mathcal{E}^{(r)})$	$\text{Corr}(J, \mathcal{E}_A^{(r)})$
0	35	0.875	7.158	1.204	0.634	0.539
1	34	0.850	7.580	1.205	0.601	0.575
2	34	0.850	7.400	1.185	0.624	0.630
3	35	0.875	7.277	1.177	0.624	0.592
4	35	0.875	8.157	1.181	0.607	0.534

**Hyperparameter robustness.** Table 5 varies dictionary size  $m$  and sparsity parameter  $\alpha$ . Certification remains high (0.85–0.90), and slack minima remain  $> 1$  in all settings. This indicates that the certificate is not tied to one specific dictionary configuration, which is essential if jamming is to be treated as a structural property of the chart rather than a modelling artefact.

Table 5: Hyperparameter robustness for Result C (40 charts). Coverage and correctness are stable across dictionary sizes and sparsity strengths.

$(m, \alpha)$	Cert. charts	Cert. rate	Slack median	Slack min	$\text{Corr}(J, \mathcal{E}^{(r)})$	$\text{Corr}(J, \mathcal{E}_A^{(r)})$
(128, 0.5)	35	0.875	6.785	1.198	0.464	0.464
(128, 1.0)	36	0.900	6.801	1.198	0.538	0.550
(256, 0.5)	34	0.850	6.746	1.204	0.497	0.477
(256, 1.0)	35	0.875	7.158	1.204	0.634	0.539
(512, 0.5)	34	0.850	7.054	1.202	0.424	0.292
(512, 1.0)	34	0.850	8.566	1.202	0.662	0.620

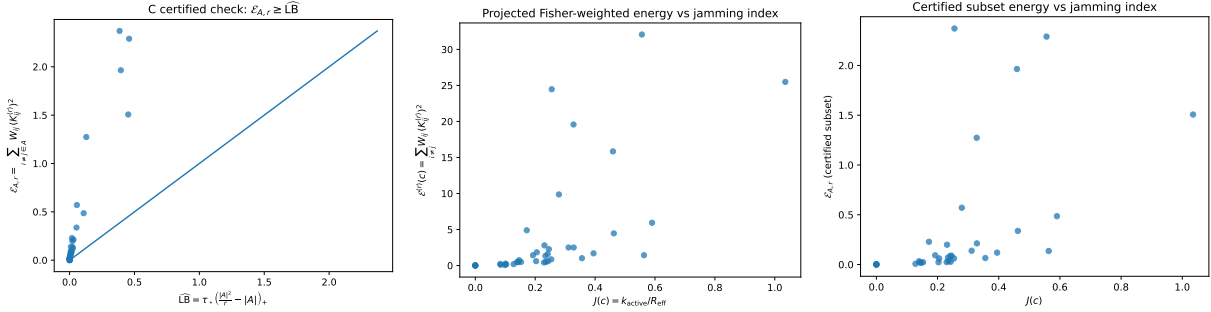


Figure 4: Result C diagnostics (PDF). Left: certificate check  $\mathcal{E}_A^{(r)} \geq \widehat{LB}$ . Middle: projected interference energy vs jamming index  $J(c)$ . Right: certified subset energy vs  $J(c)$ .

**Figure interpretation (certificate and correlation diagnostics).** Figure 4 contains three plots that answer three distinct questions:

1. *Certificate check:*  $\mathcal{E}_A^{(r)}$  vs  $\widehat{LB}$ . Points must lie above the diagonal; this confirms the inequality numerically for all certified charts.
2. *Projected energy vs jamming:* tests whether  $J(c)$  tracks the measured interference energy on the bandwidth-projected subspace.
3. *Certified energy vs jamming:* tests the same relationship restricted to the consequential subset used for certification.

Together they show both that the certificate holds and that the jamming index has predictive value as an interference proxy.

### 9.5 D: stability of $D_{\text{shear}}$ and $D_{\text{hol}}$ under resampling

Result D is about estimator behaviour under finite overlap sampling. We use bootstrap resampling to quantify variability when overlap sets are resampled with replacement Efron (1992). We report (i) global bootstrap summaries across many edges/loops and (ii) within-edge and within-loop sample-size curves that isolate concentration with increasing  $n_{\text{boot}}$ .

**Global bootstrap summary (distributional stability).** We bootstrap  $D_{\text{shear}}$  and  $D_{\text{hol}}$  by resampling overlap sets with replacement.

For  $D_{\text{shear}}$ , each bootstrap replicate resamples  $n_{\text{boot}}$  overlap points per selected edge and recomputes  $Q_{vu} = \text{polar}(\widehat{T}_{vu})$  and  $\widehat{P}_{vu} = \text{polar}(B_v^\top B_u)$ , yielding  $D_{\text{shear}}(u, v) = \|Q_{vu} - \widehat{P}_{vu}\|_F / (2\sqrt{k})$ .

For  $D_{\text{hol}}$ , we sample fundamental cycles induced by chords in a spanning tree of the LCC: for each chord  $(u, v)$  we close the unique tree path from  $u$  to  $v$  with the chord step  $v \rightarrow u$ . In each replicate we estimate the required per-edge  $(Q_{vu}, \widehat{P}_{vu})$  from resampled overlaps, form  $g_{vu} = \widehat{P}_{vu}^\top Q_{vu}$ , then compute the loop product  $h_\gamma = \prod g$  and  $D_{\text{hol}}(\gamma) = \|h_\gamma - I\|_F / \sqrt{2k}$ . Because overlap sizes vary by edge, some replicate-cycle evaluations may be undefined if one or more cycle edges lack sufficient overlap; the reported global holonomy statistics therefore aggregate only those replicate-cycle evaluations for which all required cycle edges were successfully estimated (hence the realised global #samples can be  $< B \times n_{\text{cycles}}$ ).

Table 6: Global bootstrap stability summaries (normalised). Each row aggregates many bootstrap replicates across sampled edges (shearing) or cycles (holonomy). Quantiles describe the distributional tails of the measured defects.

Subsystem	Metric	#samples	mean	std	q05	q50	q95
Baseline	$D_{\text{shear}}$	10000	0.2403	0.0689	0.0966	0.2463	0.3334
Baseline	$D_{\text{hol}}$	1200	0.5772	0.0977	0.4277	0.5777	0.7386
Persistent ( $s_{\text{min}} = 0.015$ )	$D_{\text{shear}}$	10000	0.2033	0.0629	0.0845	0.2104	0.2951
Persistent ( $s_{\text{min}} = 0.015$ )	$D_{\text{hol}}$	4200	0.5454	0.1355	0.3875	0.5038	0.8018

**Within-edge concentration (estimator variance at fixed edge).** Tables 7 and 8 fix a single edge and vary  $n_{\text{boot}}$ . This isolates estimator concentration: the standard deviation in Table 8 decreases from 0.00606 at  $n = 256$  to 0.00169 at  $n = 2736$ , which is consistent with Lemma 7.1 (better conditioning implies smaller variability of polar factors and therefore of  $D_{\text{shear}}$ ).

Table 7: Within-edge stability for  $D_{\text{shear}}$  on baseline edge (3-33),  $B = 200$ .

$n_{\text{boot}}$	mean $D_{\text{shear}}$	std
256	0.69348	0.00760
512	0.70326	0.00515
1024	0.70058	0.00588
2000	0.70735	0.00537
4000	0.70086	0.00824

Table 8: Within-edge stability for  $D_{\text{shear}}$  on persistent edge (68-83),  $B = 200$  (last row capped by available overlap). The decreasing std indicates concentration with increasing overlap size.

$n_{\text{boot}}$	mean $D_{\text{shear}}$	std
256	0.07365	0.00606
512	0.05668	0.00394
1024	0.04654	0.00247
2000	0.04146	0.00193
2736	0.03994	0.00169

**Within-loop concentration (cycle-level stability).** Tables 9 and 10 fix a single fundamental cycle and vary  $n_{\text{boot}}$ . The standard deviation remains on the order of  $2 \times 10^{-2}$  to  $3 \times 10^{-2}$ , which is expected because holonomy aggregates multiple edges (Lemma 7.2). The mean values stabilise after  $n = 512$  in both examples, supporting that  $D_{\text{hol}}$  is not a fragile artefact of a particular overlap subsample.

Table 9: Within-loop stability for  $D_{\text{hol}}$  on a baseline fundamental cycle (chord 40–102),  $B = 200$ .

$n_{\text{boot}}$	mean $D_{\text{hol}}$	std
256	0.48596	0.03030
512	0.44759	0.02893
1024	0.44692	0.02899
2000	0.44595	0.02749
4000	0.44489	0.02925

Table 10: Within-loop stability for  $D_{\text{hol}}$  on a persistent fundamental cycle (chord 71–96),  $B = 200$ .

$n_{\text{boot}}$	mean $D_{\text{hol}}$	std
256	0.56800	0.02492
512	0.54174	0.02157
1024	0.52724	0.02404
2000	0.52747	0.02169
4000	0.52957	0.02452

**Conclusion for D.** Across both edge-level and loop-level tests, the reported diagnostics stabilise under resampling at practical overlap sizes. Persistent filtering improves within-edge concentration, consistent with polar-factor perturbation theory.

## 10 Obstructions and atlas-level summaries

**Definition 10.1** (Three geometric obstructions). **O1: Local jamming:** large  $J(c) = k_{\text{active}}(c)/R_{\text{eff}}(G^{(c)})$  indicates load exceeds bandwidth.

**O2: Proxy shearing:** large  $D_{\text{shear}}(u, v)$  implies unavoidable mismatch by Theorem 4.2.

**O3: Nontrivial holonomy:** large  $D_{\text{hol}}(\gamma)$  obstructs global trivialisation by Theorem 5.2.

Atlas-level aggregates can be reported as means and quantiles:

$$\mathcal{J}_{\text{atlas}} = \mathbb{E}_c[J(c)], \quad \mathcal{S}_{\text{atlas}} = \mathbb{E}_{(u,v)}[D_{\text{shear}}(u, v)], \quad \mathcal{H}_{\text{atlas}} = \mathbb{E}_\gamma[D_{\text{hol}}(\gamma)].$$

In this paper, the emphasis is on establishing that the edge and loop diagnostics are well-defined, certified when claimed, and stable under resampling.

## 11 Limitations

- Correspondence-proxy dependence.**  $\hat{P}_{vu}$  is a proxy; conclusions about “mismatch” are conditional on the proxy definition.
- Transport model class.** We use linear transports on overlap codes; nonlinear transports may be required for certain strata.
- No topological overclaim.** Nontrivial holonomy obstructs a connection-compatible trivialisation under the learned transports (with respect to the fixed correspondence proxy); it does not prove topological nontriviality of an underlying continuous bundle.
- Scaling constraints.** Full Fisher matrices can be expensive; scalable variants (diagonal/block/low-rank) should be used for large  $m_c$ .

---

## 12 Conclusion

We presented a discrete gauge-theoretic atlas formalism for superposition in LLMs and grounded it in four results with concrete empirical instantiations. Result A establishes a constructive gauge identity connecting chord residuals to holonomy, making holonomy computable and gauge-invariant. Result B turns proxy shearing into an unavoidable transfer mismatch bound. Result C provides a non-vacuous certified interference bound on consequential atom subsets with high coverage and zero violations across seeds/hyperparameters. Result D shows that the central diagnostics are stable under resampling and concentrate with overlap size, particularly on persistent subsystems. Together, these results support interpretability as an atlas construction problem with measurable local and global obstructions.

### Broader Impact Statement

This paper introduces a new mathematical and empirical framework for mechanistic interpretability: a gauge- and sheaf-theoretic *atlas* view of neural representations that replaces the common “single global dictionary” premise with a structured local-to-global objective. The core impact is conceptual and methodological: we define measurable geometric obstructions to global interpretability (local jamming, proxy shearing, and nontrivial holonomy), provide constructive gauge computations that make holonomy directly computable, and supply certified and stability-tested diagnostics that can be applied to frozen models. If adopted, this framework can change how interpretability research formulates its goals (from global feature discovery to atlas construction), and it can enable more rigorous evaluation of when and why interpretability methods fail due to context dependence, interference, and path-dependent transport.

As with most interpretability work, these tools are dual-use. They can be used to audit, debug, and improve model transparency, but they may also help an adversary identify representation regimes with large mismatch or curvature and exploit them to induce or amplify undesirable behaviours. The paper does not introduce new training procedures or increase model capability; it provides analysis tools and measurements on an existing frozen model. Responsible use includes applying these diagnostics to safety evaluation and robustness testing, and exercising caution when publishing fine-grained analyses that might facilitate targeted attacks.

### Author Contributions

Hossein Javidnia conceived the study; developed the theoretical framework; designed and implemented the experimental pipeline; conducted the experiments; analysed and interpreted the results; and wrote the manuscript.

### Acknowledgments

The author thanks the ADAPT Centre for providing access to high-performance computing (HPC) resources used for the experimental runs. The ADAPT Centre did not contribute to the study design, analysis, interpretation, or writing.

### References

- Shun-ichi Amari. *Information Geometry and Its Applications*, volume 194 of *Applied Mathematical Sciences*. Springer, 2016. doi: 10.1007/978-4-431-55978-8.
- Leonard Bereska and Efstratios Gavves. Mechanistic interpretability for ai safety—a review. *arXiv preprint arXiv:2404.14082*, 2024.
- Cristian Bodnar, Francesco Di Giovanni, Benjamin Chamberlain, Pietro Lio, and Michael Bronstein. Neural sheaf diffusion: A topological perspective on heterophily and oversmoothing in gnns. *Advances in Neural Information Processing Systems*, 35:18527–18541, 2022.
- Trenton Bricken, Adly Templeton, Joshua Batson, Brian Chen, Adam Jermyn, Tom Conerly, Nicholas L. Turner, Cem Anil, Carson Denison, Amanda Askell, Robert Lasenby, Yifan Wu, Shauna Kravec, Nicholas Schiefer, Tim Maxwell, Nicholas Joseph, Alex Tamkin, Karina Nguyen, Brayden McLean, Josiah E. Burke,

- 
- Tristan Hume, Shan Carter, Tom Henighan, and Christopher Olah. Towards monosemanticity: Decomposing language models with dictionary learning, October 2023. URL <https://transformer-circuits.pub/2023/monosemantic-features>. Transformer Circuits Thread.
- Ole Christensen et al. *An introduction to frames and Riesz bases*, volume 7. Springer, 2003.
- Arthur Conmy, Augustine Mavor-Parker, Aengus Lynch, Stefan Heimersheim, and Adrià Garriga-Alonso. Towards automated circuit discovery for mechanistic interpretability. In A. Oh, T. Naumann, A. Globerson, K. Saenko, M. Hardt, and S. Levine (eds.), *Advances in Neural Information Processing Systems*, volume 36, pp. 16318–16352. Curran Associates, Inc., 2023.
- Justin Michael Curry. *Sheaves, cosheaves and applications*. University of Pennsylvania, 2014.
- Bradley Efron. Bootstrap methods: another look at the jackknife. In *Breakthroughs in statistics: Methodology and distribution*, pp. 569–593. Springer, 1992.
- Nelson Elhage, Tristan Hume, Catherine Olsson, Nicholas Schiefer, Tom Henighan, Shauna Kravec, Zac Hatfield-Dodds, Robert Lasenby, Dawn Drain, Carol Chen, Roger Grosse, Sam McCandlish, Jared Kaplan, Dario Amodei, Martin Wattenberg, and Christopher Olah. Toy models of superposition. 2022. URL <https://arxiv.org/abs/2209.10652>.
- Jakob Hansen and Robert Ghrist. Toward a spectral theory of cellular sheaves. *Journal of Applied and Computational Topology*, 3(4):315–358, 2019.
- Nicholas J. Higham. Computing the polar decomposition—with applications. *SIAM Journal on Scientific and Statistical Computing*, 7(4):1160–1174, 1986. doi: 10.1137/0907079.
- Arthur E Hoerl and Robert W Kennard. Ridge regression: Biased estimation for nonorthogonal problems. *Technometrics*, 12(1):55–67, 1970.
- Ian Jolliffe. Principal component analysis. *Encyclopedia of statistics in behavioral science*, 2005.
- Denis Kocetkov, Raymond Li, Loubna Ben Allal, Jia Li, Chenghao Mou, Carlos Muñoz Ferrandis, Yacine Jernite, Margaret Mitchell, Sean Hughes, Thomas Wolf, et al. The stack: 3 tb of permissively licensed source code. *arXiv preprint arXiv:2211.15533*, 2022.
- James Martens and Roger Grosse. Optimizing neural networks with kronecker-factored approximate curvature. In *International conference on machine learning*, pp. 2408–2417. PMLR, 2015.
- James B McQueen. Some methods of classification and analysis of multivariate observations. In *Proc. of 5th Berkeley Symposium on Math. Stat. and Prob.*, pp. 281–297, 1967.
- Stephen Merity, Caiming Xiong, James Bradbury, and Richard Socher. Pointer sentinel mixture models. *arXiv preprint arXiv:1609.07843*, 2016.
- Meta. meta-llama/llama-3.2-3b-instruct (model card), September 2024. URL <https://huggingface.co/meta-llama/Llama-3.2-3B-Instruct>. Hugging Face model card page.
- Colin Raffel, Noam Shazeer, Adam Roberts, Katherine Lee, Sharan Narang, Michael Matena, Yanqi Zhou, Wei Li, and Peter J Liu. Exploring the limits of transfer learning with a unified text-to-text transformer. *Journal of machine learning research*, 21(140):1–67, 2020.
- André Ribeiro, Ana Luiza Tenório, Juan Belieni, Amauri H Souza, and Diego Mesquita. Cooperative sheaf neural networks. *arXiv preprint arXiv:2507.00647*, 2025.
- Peter H. Schönemann. A generalized solution of the orthogonal procrustes problem. *Psychometrika*, 31(1): 1–10, 1966. doi: 10.1007/BF02289451.
- Vasileios Sevetlidis and George Pavlidis. Gauge-invariant representation holonomy. *arXiv preprint arXiv:2601.21653*, 2026.

---

Amit Singer. Angular synchronization by eigenvectors and semidefinite programming. *Applied and computational harmonic analysis*, 30(1):20–36, 2011.

Adly Templeton, Tom Conerly, Jonathan Marcus, Jack Lindsey, Trenton Bricken, Brian Chen, Adam Pearce, Craig Citro, Emmanuel Ameisen, Andy Jones, Hoagy Cunningham, Nicholas L. Turner, Callum McDougall, Monte MacDiarmid, C. Daniel Freeman, Theodore R. Sumers, Edward Rees, Joshua Batson, Adam Jermyn, Shan Carter, Christopher Olah, and Tom Henighan. Scaling monosemanticity: Extracting interpretable features from claude 3 sonnet, May 2024. URL <https://transformer-circuits.pub/2024/scaling-monosemanticity/>. Transformer Circuits Thread.

Lloyd Welch. Lower bounds on the maximum cross correlation of signals (corresp.). *IEEE Transactions on Information theory*, 20(3):397–399, 1974.